Inverse modeling of Texas NO_x emissions using space-based and ground-based NO_2 observations

Wei Tang[1,*], Daniel Cohan[1], Lok N. Lamsal[2,3], Xue Xiao[1], Wei Zhou[1]

[1]*Department of Civil and Environmental Engineering, Rice University, 6100 Main Street MS 519, Houston, TX 77005, USA; Email: Wei.Tang@rice.edu*

[2]*NASA Goddard Space Flight Center, Greenbelt, MD, USA*

[3]*Goddard Earth Sciences Technology & Research, Universities Space Research Association, Columbia, MD, USA*

Supporting Information

1. Meteorological parameters evaluations

The MM5 modeled hourly temperature, wind speed, and wind direction are evaluated with measured data from 34 ground monitoring sites over the 12km CAMx domain for both modeling episodes (Table S1). The model simulates the temperature and wind speed well, showing that the mean bias error (MBE) is less than 0.5K and the root mean square error (RMSE) is less than 2K for the temperature, and the MBE and RMSE are around 2 m/s for the wind speed, which are similar to evaluation results from the study done by Kim et al. (2011). The simulated wind direction shows slightly weak performance in terms of RMSE. However, according to TCEQ (2010 and 2011), the large discrepancy between observed and modeled wind directions mostly occurred with very low wind speed, thus, it only has slight influence on the CAMx modeling.

Modeled PBL heights are evaluated with available measurement data from two sites at Huntsville airport, Huntsville, TX (30.75°N, 95.58°W) and Jefferson airport, Port Arthur, TX (29.94°N, 94.00°W) for the June episode (Fig. S1), and from three sites at Huntsville airport, Jefferson airport, and LaPorte airport, La Porte, TX (29.67°N, 95.06°W) for the August-September episode (Fig. S2). The model overpredicts the daytime PBL height for the June

episode with exceptions at 8am and 7pm in the Huntsville site and 8am at Jefferson site (Fig. S1), while the August-September episode tends to underpredict PBL heights at Huntsville and Jefferson sites, but it shows a good agreement with measurement at LaPorte site (Fig. S2). The overprediction of PBL heights in the June episode, but underprediction of that in the August-September episode is probably caused by using different vertical mixing schemes in the MM5 modeling. The June episode uses ACM2 vertical mixing scheme to simulate PBL heights which tends to have stronger mixing (Pleim 2007).

2. Sensitivity analysis of the DKF inversions

Sensitivity tests by varying uncertainty values in the error covariance matrices for both OMI-based and ground-based DKF inversions in the actual inversion case are performed (Fig. S3). The results are very similar to the pseudodata test: the adjustments for the posteriors are insensitive to the emission error covariance matrix, and slightly responsive to the assumed observation errors.

3. Direct Scaling (DS) inversion

3.1 Method

The DS method applies the ratio between satellite NO_2 observations and modeled NO_2 concentrations to scale the bottom-up NO_x emissions in each grid cell:

$$E_t = E_b \times \frac{\Omega_s}{\Omega_m} \qquad \text{(S1)}$$

where E_t is the top-down NO_x emission rate; E_b is the bottom-up NO_x emission rate; Ω_s and Ω_m are the satellite and modeled NO_2 column densities, respectively.

This method was developed in a global model with coarse grid resolution and assumes that the NO_2 concentration in each model grid will not be affected by the NO_x emitted from surrounding grids. However, in a regional model with relatively small grid size, this assumption may fail, generating a spatial smearing error when NO_x lifetime is longer than the horizontal transport time (Martin et al., 2003; Boersma et al., 2008; Lamsal et al., 2010; Turner et al., 2012). Martin et al. (2003) indicated that the spatial smearing error can be neglected if the grid length is greater than 100km. Therefore, smoothing kernels (Toenges-Schuller et al., 2006; Boersma et al., 2008; Lamsal et al., 2010) need to be applied in order to alleviate the spatial smearing error in CAMx by accounting for the emissions from adjacent grid cells in developing the top-down NO_x emissions. The smoothing kernel is defined as

$$K = \frac{1}{k+8}\begin{pmatrix} 1 & 1 & 1 \\ 1 & k & 1 \\ 1 & 1 & 1 \end{pmatrix} \quad \text{(S2)}$$

where k is a smoothing parameter, and is determined by applying the smoothing kernel (K) to each grid cell in the bottom-up NO_x emission inventory with different k values until the correlation between smoothed bottom-up NO_x emissions and corresponding CAMx modeled NO_2 column density reaches a maximum. The smoothing kernel (K) is then applied to Eq. (S1) to form Eq. (S3),

$$E^t_{i,j} = \frac{E^b_{i,j}}{\sum_{n=-1}^{1}\sum_{l=-1}^{1} K_{l,n} E^b_{i+l,j+n}} \frac{\Omega_s}{\Omega_{\mathrm{m}}} \times E^b_{i,j} \quad \text{(S3)}$$

where i and j represent column and row in horizontal model grids.

3.2 Results

The DS inversion method was performed with OMI NO_2 column densities to create top-down NO_x emissions for the 12-km modeling domain. The monthly averaged (June 3 to July 1, and August 16 to September 15) NO_2 column densities at 1-2pm were used to calculate the ratio of OMI to CAMx (Eq. S1). The first three modeling days were discarded for both modeling episodes to avoid the influence of initial conditions. The monthly 24-h averaged NO_x emissions and modeled NO_2 column densities were used to determine the value of the smoothing parameter, *k*. In this case, *k* equals to 2.0 for both episodes, indicating large influence of NO_x emissions transported from surrounding grid cells.

Results (Table S2) show the DS inversion scales up the NO_x emissions in all seven regions, leading to higher estimates of modeled NO_2 column densities (Figs. S4) in most of the domain. However, especially in urban areas, the simulated NO_2 column densities with inverted NO_x emissions overshoot those observed by OMI. This indicates that the ability of NO_x to influence its own lifetime via changes in OH radical concentrations results in significant nonlinearity between NO_2 concentration and NO_x emission that are neglected by the DS method. Use of inverted NO_x emissions does reduce bias and error in simulating OMI observed column densities, while R^2 gets worse (Table S3), indicating no improvement in the spatial distribution. The comparisons with AQS ground NO_2 (Table S4) and O_3 (Table S5) measurements indicate that the inverted NO_x emissions actually deteriorate both simulations of ground-level NO_2 and O_3, with bias and error increasing by 70% against measured NO_2, and with bias and error increasing by 10% against measured O_3. Similar results are shown in evaluating model performance against P-3 NO_2 and NO_y measurements (Table S6): the DS inversion increases bias and error by

approximately 30% and 20%, respectively, in simulating P-3 NO_2, and around 70% and 60%, respectively, in simulating P-3 NO_y.

References

Boersma, K. F., Jacob, D. J., Bucsela, E. J., Perring, A. E., Dirksen, R., van der A, R. J., Yantosca, R. M., Park, R. J., Wenig, M. O., Bertram, T. H., and Cohen, R. C.: Validation of OMI tropospheric NO_2 observations during INTEX-B and application to constrain NO_x emissions over the eastern United States and Mexico. Atmos. Environ., 42, 4480–4497, 2008.

Lamsal, L. N., Martin, R. V., van Donkelaar, A., Celarier, E. A., Bucsela, E. J., Boersma, K. F., Dirksen, R., Luo, C., and Wang. Y.: Indirect validation of tropospheric nitrogen dioxide retrieved from the OMI satellite instrument: Insight into the seasonal variation of nitrogen oxides at northern midlatitudes. J. Geophys. Res., 115, D05302, doi:10.1029/2009JD013351, 2010.

Martin, R. V., Jacob, D. J., Chance, K., Kurosu, T. P., Palmer, P. I., and Evans, M. J.: Global inventory of nitrogen oxide emissions constrained by space-based observations of NO_2 columns. J. Geophys. Res.**,** 108(D17), 4537, doi:10.1029/2003JD003453, 2003.

Kim, S.-W., McKeen, S. A., Frost, G. J., Lee, S.-H., Trainer, M., Richter, A., Angevine, W.M., Atlas, E., Bianco, L., Boersma, K. F., Brioude, J., Burrows, J. P., de Gouw, J., Fried, A., Gleason, J., Hilboll, A., Mellqvist, J., Peischl, J., Richter, D., Rivera, C., Ryerson, T., te Lintel Hekkert, S., Walega, J., Warneke, C., Weibring, P., and Williams, E.: Evaluations of NO_x and highly reactive VOC emission inventories in Texas and their implications for ozone plume simulations during the Texas Air Quality Study 2006. Atmos. Chem. Phys., 11, 11361-11386, 2011.

Pleim, J.E.: A combined local and nonlocal closure model for the atmospheric boundary layer. Part II: Application and evaluation in a mesoscale meteorological model. J. Appl. Meteorol. Clim., 46, 1396-1408, 2007.

TCEQ.: Houston-Galveston-Brazoria Attainment Demonstration SIP Revision for the 1997 Eight-Hour Ozone Standard, Austin, TX, 2010.

TCEQ.: Dallas-Fort Worth Attainment Demonstration SIP Revision for the 1997 Eight-hour Ozone Standard Non-attainment Area, Austin, TX, 2011.

Toenges-Schuller, N., Stein, O., Rohrer, F., Wahner, A., Richter, A., Burrows, J. P., Beirle, S., Wagner, T., Platt, U., and Elvidge, C. D.: Global distribution pattern of anthropogenic nitrogen oxide emissions: Correlation analysis of satellite measurements and model calculations. J. Geophys. Res., 111, D05312, doi:10.1029/2005JD006068, 2006.

Turner, A., Henze, D. K., Martin, R. V., and Hakami, A.: The spatial extent of source influences on modeled column concentrations of short-lived species. Geophys. Res. Lett., 39, L12806, doi:10.1029/2012GL051832, 2012.

Table S1. Evaluation of MM5 in simulating hourly temperature, wind speed and wind direction from 34 ground monitoring sites for both June and Aug-Sep episodes.

Parameters	June 3 to July 1, 2006			August 16 to September 15, 2006		
	T (K)	Wind Speed (m/s)	Wind Direction (°)	T (K)	Wind Speed (m/s)	Wind Direction (°)
MBE[a]	0.22	1.76	-4.00	0.21	1.99	-13.73
RMSE[b]	1.58	2.13	96.72	1.87	2.28	112.65

a. Mean bias error
b. Root mean square error

Table S2. Scaling factors for each region from DS inversions.

Source Region	June 3 to July 1, 2006			August 16 to September 15, 2006		
	Base NO_X emission (tons/day)	Priori NO_X emission[a] (tons/day)	Scaling factor relative to priori (unitless)	Base NO_X emission (tons/day)	Priori NO_X emission (tons/day)	Scaling factor relative to priori (unitless)
			Posteriori OMI-based DS inversion			Posteriori OMI-based DS inversion
HGB	374	455	1.46	382	436	1.56
DFW	335	435	1.36	314	412	1.47
BPA	81	97	2.23	86	98	2.02
NE Texas	141	164	2.33	155	174	1.69
Austin and San Antonio	252	319	1.55	248	302	1.82
N rural	522	823	1.93	543	759	2.00
S rural	472	728	1.83	489	668	2.04

a. Adds lightning and aircraft NO_x, and doubled soil NO_x emissions to the base case

Table S3. Performance of CAMx in simulating OMI-observed NO_2 column densities.

Statistical Parameters	June 3 to July 1, 2006			August 16 to September 15, 2006		
	Base case	Priori[c]	Posteriori OMI-based DS inversion	Base case	Priori	Posteriori OMI-based DS inversion
R^2	0.62	0.61	0.42	0.63	0.48	0.40
NMB[a]	-0.47	-0.30	0.087	-0.54	-0.33	0.13
NME[b]	0.48	0.32	0.22	0.55	0.39	0.32

a. Normalized mean bias
b. Normalized mean error
c. Adds lightning and aircraft NO_x, and doubled soil NO_x emissions to the base case

Table S4. Performance of CAMx in simulating AQS hourly ground-level NO_2.

Statistical Parameters	June 3 to July 1, 2006			August 16 to September 15, 2006		
	Base case	Priori	Posteriori OMI-based DS inversion	Base case	Priori	Posteriori OMI-based DS inversion
R^2	0.56	0.56	0.50	0.52	0.52	0.45
NMB	0.89	0.98	1.76	0.42	0.49	1.20
NME	1.01	1.09	1.80	0.66	0.71	1.29

Table S5. Performance of CAMx in simulating AQS hourly ground-level O_3.

Statistical Parameters	June 3 to July 1, 2006		August 16 to September 15, 2006	
	Priori	Posteriori OMI-based DS inversion	Priori	Posteriori OMI-based DS inversion
R^2	0.61	0.61	0.50	0.52
NMB	0.01	0.12	0.38	0.49
NME	0.29	0.37	0.47	0.58

Table S6. Performance of CAMx in simulating P-3 aircraft-observed NO_2 and NO_y.

Statistical Parameters	NO_2[a]			NO_y[a]		
	Base case	Priori	Posteriori OMI-based DS inversion	Base case	Priori	Posteriori OMI-based DS inversion
R^2	0.23	0.23	0.25	0.34	0.34	0.36
NMB	0.10	0.10	0.46	0.65	0.68	1.41
NME	0.99	0.99	1.24	0.94	0.97	1.54

a. Comparison available for only four days (August 31, September 11, September 13, and September 15, 2006).

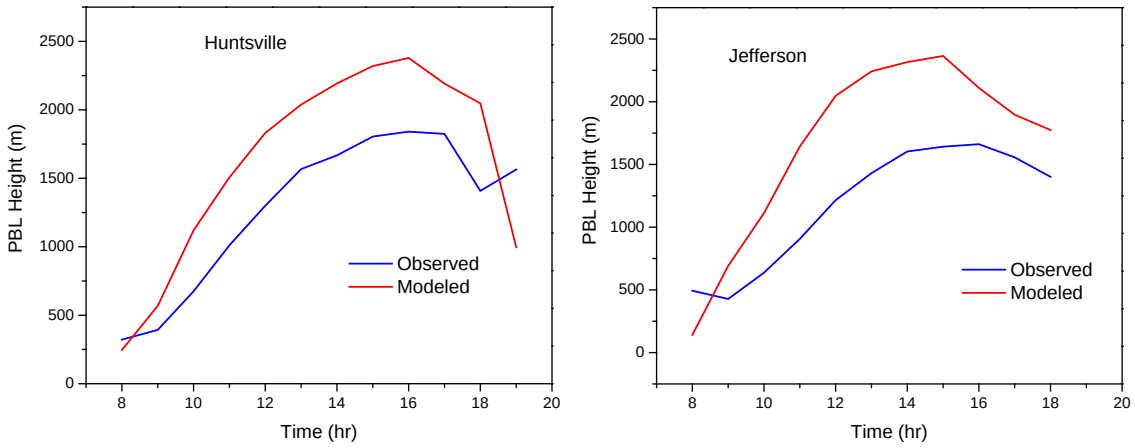

Figure S1. Temporal variations of monthly averaged modeled and measured PBL heights at Huntsville airport (30.75°N, 95.58°W) and Jefferson airport (29.94°N, 94.00°W).

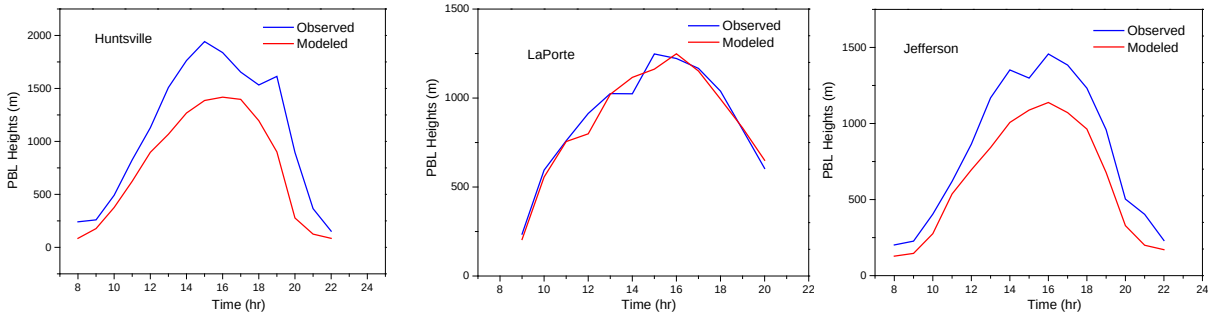

Figure S2. Temporal variations of monthly averaged modeled and measured PBL heights at Huntsville airport (30.75°N, 95.58°W), LaPorte airport (29.67°N, 95.06°W), and Jefferson airport (29.94°N, 94.00°W).

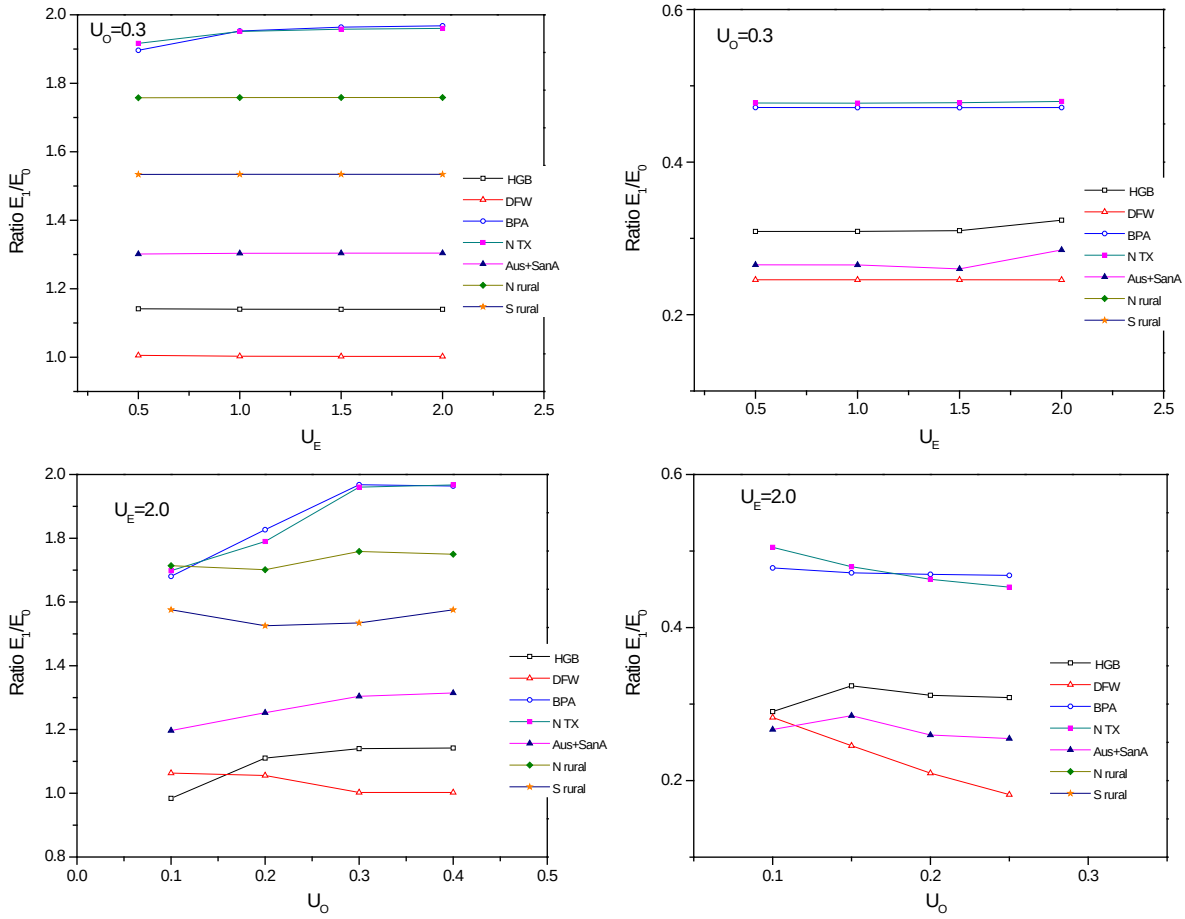

Figure S3. Sensitivity analysis of Kalman filter inversion by changing emission uncertainties (top), and observation uncertainties (bottom) using OMI NO_2 (left) and AQS ground NO_2 (right).

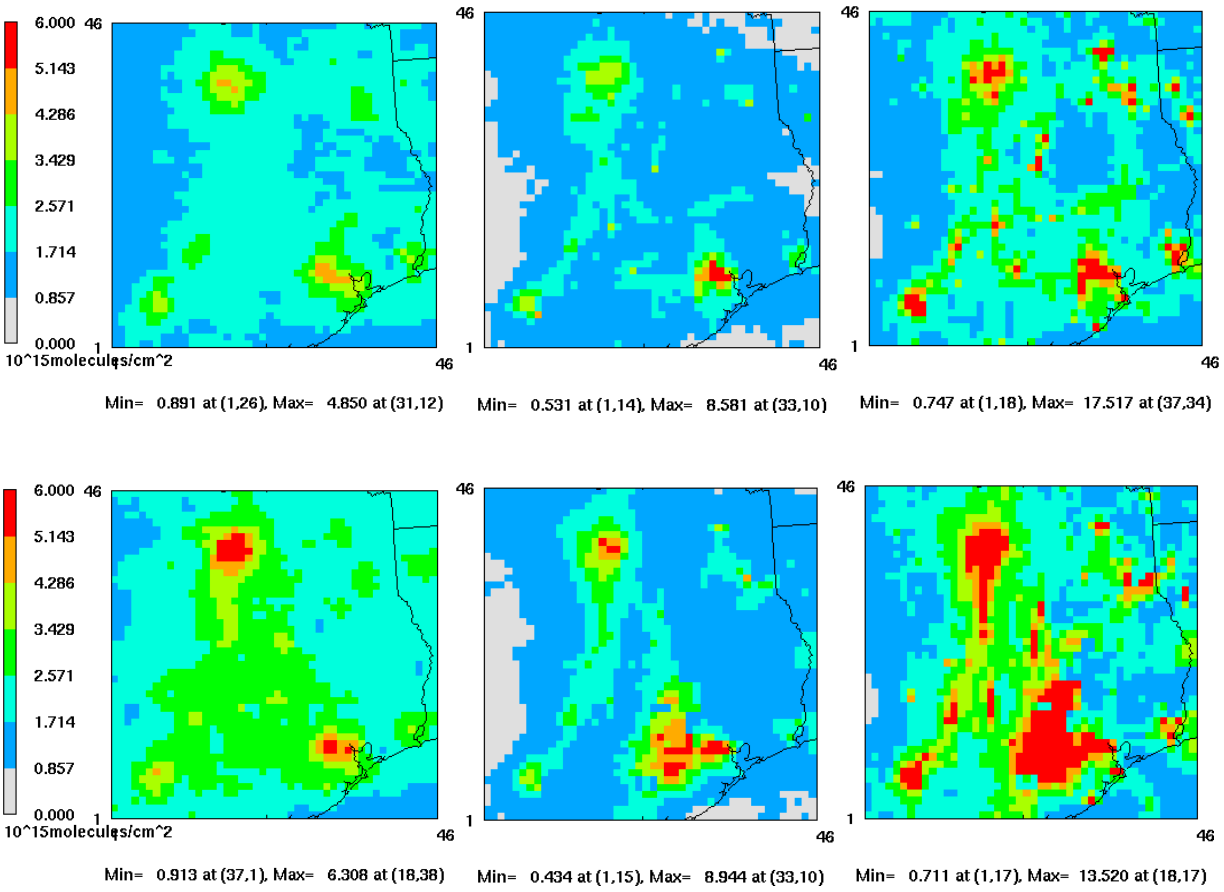

Figure S4. Monthly averaged tropospheric NO_2 vertical columns at 1-2pm from OMI observations (left), and from CAMx simulations using a priori NO_x emissions (middle) and DS method inverted NO_x emissions for both June (top) and August-September episode.